# Simultaneously Enhancing the Dynamic Damping and Static Strength Capabilities of Structures: A Case Study Conducted on Fly Ash-based Geopolymer Concrete Specimens using Modal, Mechanical and Microstructural Investigations

**Ferhat Çeçen[1], Ahmet Özbayrak[2*], Bekir Aktaş[3]**

[1] Göller Bölgesi Teknokent Coordinatorship, Süleyman Demirel University, Isparta, Türkiye
[2, 3] Department of Civil Engineering, Faculty of Engineering, Erciyes University, Kayseri, Türkiye
[1] cecenferhat@sdu.edu.tr, [*2] ozbayrak@erciyes.edu.tr, [3] baktas@erciyes.edu.tr

**Abstract:** Enhancing both the dynamic damping and static strength of ordinary Portland cement (OPC) concrete simultaneously is a significant challenge. Geopolymer concrete (GPC), particularly fly ash-based GPC, offers a promising alternative. This study explores the relationship between damping and strength in heat-cured, low-calcium fly ash-based GPC using sodium silicate (SS) and sodium hydroxide (SH) activators. The findings reveal that SS activators demonstrate stronger positive correlations between damping and strength compared to SH activators. Microstructural analysis indicated that increasing SS dosage from 55 kg/m³ to 98 kg/m³ resulted in a 17% increase in dynamic damping ratios and a 39% increase in static compressive strength. These results highlight the potential of GPC to surpass OPC concrete in applications requiring both enhanced damping and strength, offering a dual benefit not typically achievable with OPC. The study contributes to a deeper understanding of GPC's capabilities, paving the way for its broader adoption in construction projects.

**Key words:** Geopolymer concrete, Microstructure, Compressive strength, Damping ratio, Resonance frequency.

## Yapıların Dinamik Sönümleme ve Statik Dayanım Yeteneklerinin Eş Zamanlı Olarak Geliştirilmesi: Uçucu Kül Esaslı Geopolimer Beton Numuneler Üzerinde Modal, Mekanik ve Mikroyapısal İncelemeler Kullanılarak Gerçekleştirilen Bir Vaka Çalışması

**Özet:** Portland çimentosu (OPC) betonu için hem dinamik sönümlemeyi hem de statik dayanımı aynı anda artırmak, önemli bir zorluktur. Geopolimer beton (GPC), özellikle uçucu kül bazlı GPC, umut verici bir alternatif sunmaktadır. Bu çalışma, düşük kalsiyumlu uçucu kül bazlı GPC'de sönümleme ve dayanım arasındaki ilişkiyi, sodyum silikat (SS) ve sodyum hidroksit (SH) aktivatörleri kullanarak araştırmaktadır. Bulgular, SS aktivatörlerinin SH aktivatörlerine kıyasla sönümleme ve dayanım arasında daha güçlü pozitif korelasyonlar gösterdiğini ortaya koymaktadır. Mikroyapı analizi, SS dozajının 55 kg/m³'ten 98 kg/m³'e artırılmasının dinamik sönümleme oranlarında %17 ve statik basınç dayanımında %39 artışa neden olduğunu göstermiştir. Bu sonuçlar, GPC'nin OPC betona kıyasla her iki özelliğin de artırılması gereken uygulamalarda üstün olma potansiyelini vurgulamakta ve OPC ile tipik olarak elde edilemeyen çift fayda sunmaktadır. Çalışma, GPC'nin yeteneklerini daha iyi anlamaya katkıda bulunarak, inşaat projelerinde daha geniş çapta benimsenmesinin önünü açmaktadır.

**Anahtar kelimeler:** Geopolimer beton, Mikroyapı, Basınç dayanımı, Sönüm oranı, Rezonans frekansı.

## 1. Introduction

Most structures inevitably experience dynamic loadings, including low-amplitude ones from vehicular traffic and human movement, as well as intense loads from large earthquakes, strong wind, and vehicle impacts [1]. Under these conditions, structural materials' dynamic characteristics and damping behaviors are, at least, just as important as their static capacities [2]. As stated in the literature, enhancement of the dynamic damping ratio, even with an increase of 10% –15%, might be a practical approach to suppressing excessive vibrations without using additional dampers or control devices [3].

Currently, during the construction of buildings or structures, one of the most preferred materials is reinforced or pre-stressed concrete. In this context, ordinary Portland cement (OPC) concrete has almost all the market share among the existing concrete types. This OPC concrete can be produced with a wide range of static compressive strength capacities. However, "higher strength" classes are needed or preferred by engineers, especially for qualified projects. Because it provides numerous benefits, such as increased static design load capabilities [4], less reinforcement usage [5], much better bond strength and decreased permeability [6], smaller concrete cross-sectional sizes [4], and higher early age strength [6]. This last advantage is especially needed for pre-stressed or prefabricated members. However, in most cases, increasing the static strength of OPC concrete also causes

---
[*] Sorumlu yazar: ozbayrak@erciyes.edu.tr. Yazarların ORCID Numarası: [1] 0000-0003-2100-8071, [2] 0000-0002-8091-4990, [3] 0000-0003-3072-7983

increases in brittleness [5], static and dynamic moduli of elasticity [7, 8], dynamic shear modulus [8], raw material costs [9], and greenhouse gas emissions [10]. Similarly, lower vibration or impact damping, lower resonance resistance [8, 11], and less sound insulation [12] can be stated as the other disadvantages of this static strength increase. Nowadays, the dynamic performance of OPC concrete can be enhanced with several methods, such as using a higher water-to-cement ratio [13, 14], lower modulus / lightweight / higher porosity aggregates (such as weathered granite, zeolite, vermiculite, etc.) [14, 15], chopped fiber reinforced polymers [16, 17], crumb rubber particles or powder [16, 18, 19], several chemical additives (such as ester copolymer emulsions, methylcellulose, air entraining agents, etc.) [14, 17, 20], and supplementary cementitious materials (SCM) (such as silica fume, fly ash, slag, and other minerals) [14, 18].

On the other hand, some of the dynamic damping performance-increasing methods mentioned above are still controversial, and there is no consensus. For example, some researchers reported contrary results for SCM materials, especially under higher frequency dynamic loads [17, 21]. The main reason for these different results is that some of the methods mentioned above do not "directly" increase the damping behavior of OPC concrete. Instead, if proper techniques are not applied, they reduce workability (because of their higher surface area), resulting in study-specific, variable results. In addition, some of them decrease the compressive strength capabilities at an early age and/or 28th day of curing. In those cases, they may cause more air gaps, less hydration development, and a weaker ITZ (interfacial transition zone). As a result, they may "indirectly" increase damping if their damping ratio-reducing effects are overcome (for example, SCM materials' filler effects & pozzolanic-reaction-induced damping ratio-lowering effects [21]. These determinations have been summarized and generalized in the literature. As stated, damping arises from the structures' or materials' elasticity, raw materials' dissipation, ITZ dimensions, solid gel structure, water-filled pores, and imperfections in the microstructure, such as voids, fractures, micro cracks, and cracks [22-24]. As seen, the factors that increase the dynamic performance are mainly the reasons that decrease the static strength. For example, a higher water-to-cement ratio provides a higher damping ratio because its internal structure and ITZ zones are more porous and have micro cracks [24, 25].

As deduced from the presented literature review, almost all of the methods that increase the dynamic damping performance of OPC concrete cannot "simultaneously" or "co-currently" increase the static compressive strengths [14, 16-18, 20]. This shortcoming of OPC concrete is still challenging for engineers, and academic investigations are continuing. Engineers are making an optimum "concrete mixture" decision in this vicious circle by sacrificing some of both the dynamic damping ratios and static compressive strengths. It is a fact that they need additional static strength-increasing methods alongside the existing dynamic performance-enhancing processes, especially for projects that require high static strength [18].

On the other hand, in recent decades, a new- generation building material named geopolymer concrete (GPC) has emerged and has been successfully used in many projects worldwide [26]. In this increasing success, its durability, high early strength, and low carbon footprint benefits played influential roles [27, 28]. Researchers have investigated many engineering properties of GPC products [26-33]. However, the available information about the dynamic (modal) characteristics of the GPC material is minimal [31-33]. Additionally, in these few studies, any relationship between the static & dynamic characteristics of GPC variations produced with variable activator types and dosages has yet to be reported. However, as deduced from the previously presented literature review, the reciprocal change behavior of "the static compressive strength and dynamic damping ratio" is crucial for structural materials.

As stated, the dynamic performance of OPC concrete can be enhanced with higher liquid ingredient dosages (higher water-to-cement ratio); however, it also causes static strength decreases [13, 14, 24, 25]. According to the literature, higher liquid ingredient (chemical activator solution) dosages also increase the damping performance of GPC [33]. However, the "co-currently increasing of the dynamic damping ratio and static compressive strength" issue has yet to be investigated for GPC variations produced with variable activator dosages. This issue was aimed at being investigated by the authors; however, any relationship between the static compressive strength and modal parameters could not be reported. Then, it was concluded that this complex relationship requires detailed and directly focused research [33].

In the production of GPC, rich-in-aluminosilicate raw materials such as slag, fly ash (FA), rice husk ash, red mud, metakaolin, silica fume, etc., are used as binder [34]. Among these aluminosilicate sources, fly ash material was preferred to be investigated in this study due to its widespread availability and significant environmental benefits. As stated in the literature, approximately one thousand million tons of FA are annually emitted by several industries and power-generating plants in the world, which causes a significant ecological problem [35]. For example, FA particles contain an essential number of heavy metals, and there is a risk of heavy metal leaching into nature if this industrial waste material is not recycled or disposed of [36]. In this context, FA-based GPC is introduced as an ideal structural material for eliminating environmental risks from FA or other hazardous wastes (wastewater, etc.) with its superior surface area, porosity, chemical resistance, mechanical strength, durability, and chemical affinity characteristics [36-39].

Unlike OPC concrete, which uses water for hydration, GPC production needs a high pH (alkaline) medium during polymerization. In this context, several chemical activators such as sodium hydroxide (SH) (NaOH), potassium hydroxide (KOH), sodium silicate (SS) ($Na_2SiO_3$), and potassium silicate ($K_2SiO_3$) are used to provide this high alkalinity [40]. Among these activators, the SS and SH activators, the most commonly used ones in the literature, were preferred to be investigated in this preliminary research study. Some researchers stated that GPC would soon be one of the most used building materials in the world if it could be produced at reasonable costs [41]. Because the high cost of chemical activators used in production hinders GPC's commercialization and extensive usage. An example of a raw material cost comparison is presented in Figure 1. This figure compares the cost of a GPC mix with that of an OPC concrete mix. The GPC and OPC concrete variations are designed with a constant binder (OPC, FA) and aggregate dosages. As seen, the current total cost of GPC is considerably (approximately %105) higher than OPC concrete, mainly due to the chemical activators. This extra cost can be partially increased or decreased by changing the types and dosages of activators.
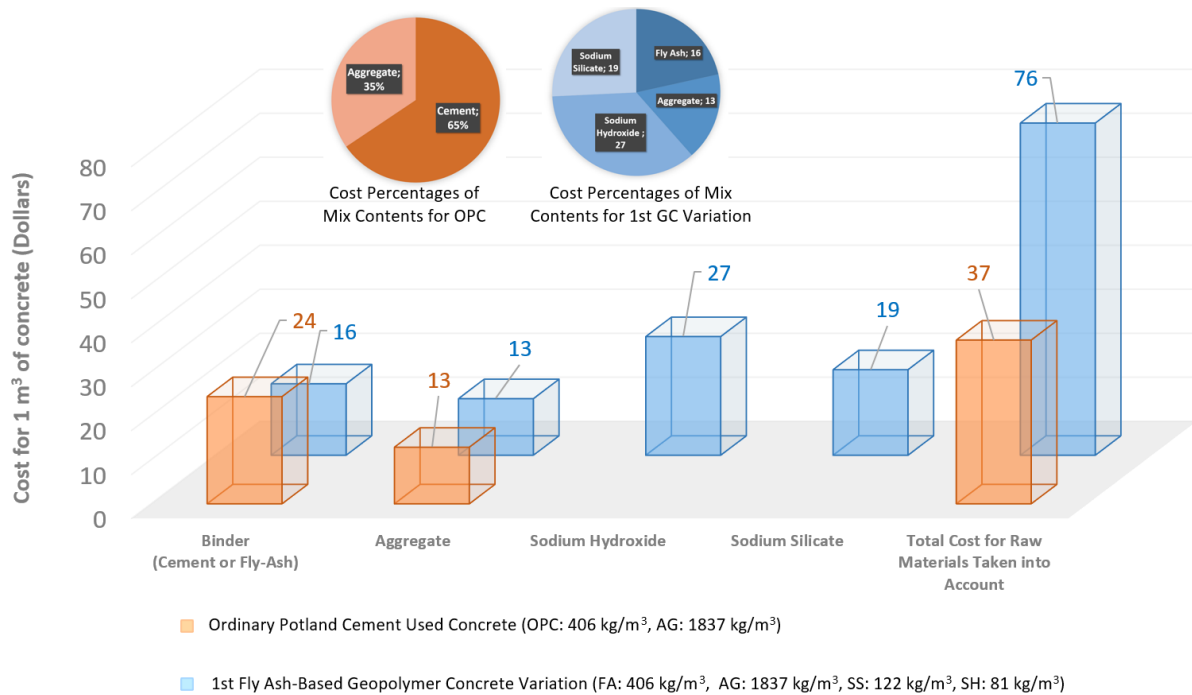


**Figure 1.** Raw material cost comparison of a GPC variation with OPC concrete (AG: Aggregate).

If the activator dosages in Figure 1 are adjusted to the values in Figure 2 the cost difference of 105% can be decreased to 86%. However, more than these saving percentages are needed to increase the GPC's commercialization and extensive usage rapidly.

As seen, the high costs of chemical activators hinder GPC's commercialization and extensive usage. On the other hand, enhancing the dynamic damping ratios and static compressive strengths of ordinary Portland cement (OPC) concrete, co-currently, is still a challenge for engineers. In this aspect, the "co-currently increasing of the dynamic damping ratio and static compressive strength" characteristic of GPC can provide a significant advantage if it exists.

This situation resembles the fact that fiber-reinforced polymer (FRP) products now have a considerable market share in the concrete reinforcing sector because of their specific advantages despite higher costs. For example, these FRP products have gained an essential share in piers, bridges, and earthquake-strengthening projects, where corrosion resistance, unit volume weight, and high mechanical strength parameters are more crucial than their higher costs. Therefore, GPC will only reflect its environmental and social benefit potentials to the field if only it is appropriately produced and used. In this context, priority should be given to the correct use of activators, which have the most significant share in production costs, and the reciprocal change of in static and dynamic characteristics of GPC specimens produced with variable activator dosages must be investigated.
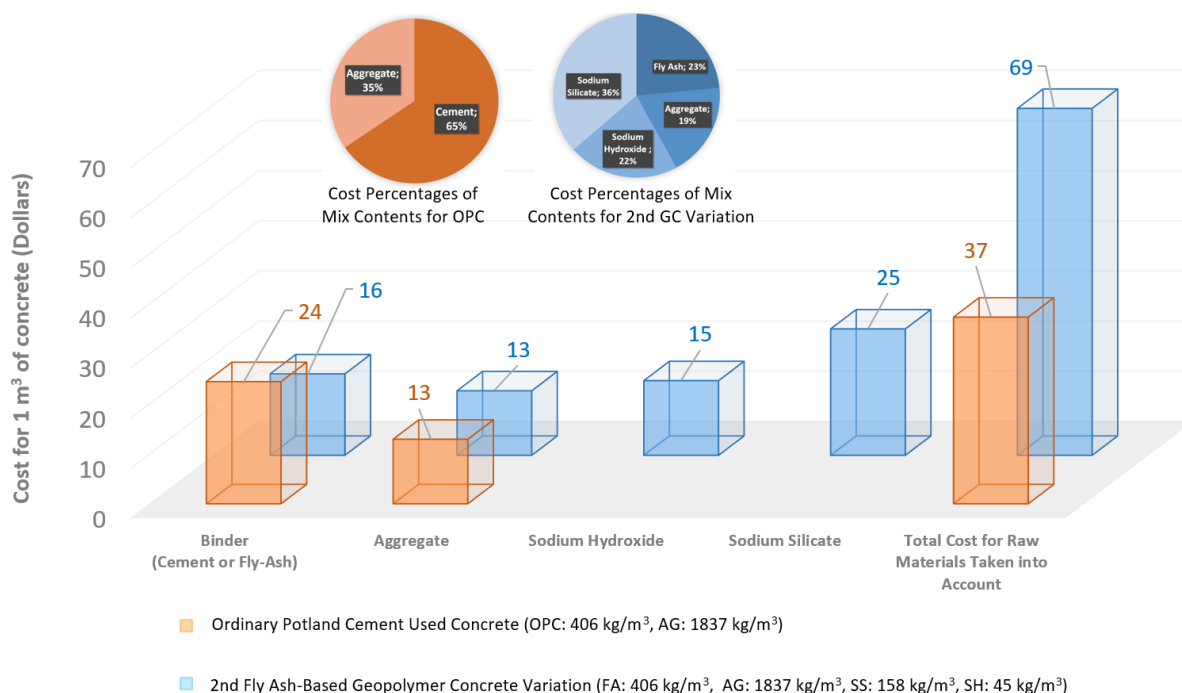
**Figure 2**. Raw material cost comparison of another GPC variation with OPC concrete.

Consequently, enhancing the dynamic damping ratios and static compressive strengths of ordinary Portland cement (OPC) concrete simultaneously remains a challenge for engineers. The potential of geopolymer concrete (GPC) to co-currently improve these properties could offer a significant advantage, yet this specific characteristic has not been thoroughly explored in the literature. Therefore, this study preliminarily investigates the effects of sodium silicate (SS) and sodium hydroxide (SH) activator solutions on the dynamic and static characteristics of fly ash-based GPC variations, aiming to address this gap and determine whether GPC can indeed provide such an advantage. During sample design, the binder (FA) and aggregate (basalt) types and dosages will remain constant for all produced specimens. And investigations will be concentrated only on the commonly used geopolymer concrete activators, the SS and SH. In addition, since this subject needs an experimental investigation from static, modal, and microstructural perspectives, all of these analyses are included in this study's scope.

## 2. Geopolymer Concrete Specimens Production

The FA used in this study was obtained from the Adana Sugözü İsken Power Plant in Türkiye. According to the X-ray fluorescence test results in Table 1, this FA is in the Class F category per ASTM C618.

**Table 1.** Chemical components of fly ash.

| Components | % | ASTM C618 Limits |
|---|---|---|
| $SiO_2$ | 55.9 | Min. 54.9% |
| Sum of $SiO_2$, $Al_2O_3$, and $Fe_2O_3$, | 85.9 | Min. 70.0 % |
| $SO_3$ | 0.33 | Max. 5.0% |
| $Na_2O$ | 1.35 | Max. 1.5% |
| LOI (loss of ignition) | 2.22 | Max. 6.0% |

**Table 2.** Mix dosages (kg/m$^3$) and several other parameters of the variations investigated in this study.

| Variation Code | FA | AG | SS | PSS | SH | PSH | AA | PA | PW | A Ratio | W Ratio |
|---|---|---|---|---|---|---|---|---|---|---|---|
| A1.5-W0.5 | 406 | 1837 | 122 | 54 | 81 | 29 | 203 | 83 | 120 | 1.5 | 0.5 |
| A1.5-W0.6 | 406 | 1837 | 146 | 64 | 97 | 35 | 243 | 99 | 144 | 1.5 | 0.6 |
| A1.5-W0.7 | 406 | 1837 | 171 | 75 | 114 | 41 | 285 | 116 | 169 | 1.5 | 0.7 |
| A2.5-W0.5 | 406 | 1837 | 145 | 64 | 58 | 21 | 203 | 85 | 118 | 2.5 | 0.5 |
| A2.5-W0.6 | 406 | 1837 | 174 | 77 | 70 | 25 | 244 | 102 | 142 | 2.5 | 0.6 |
| A2.5-W0.7 | 406 | 1837 | 203 | 89 | 81 | 29 | 284 | 118 | 166 | 2.5 | 0.7 |
| A3.5-W0.5 | 406 | 1837 | 158 | 70 | 45 | 16 | 203 | 86 | 117 | 3.5 | 0.5 |
| A3.5-W0.6 | 406 | 1837 | 189 | 83 | 54 | 19 | 243 | 102 | 141 | 3.5 | 0.6 |
| A3.5-W0.7 | 406 | 1837 | 221 | 97 | 63 | 23 | 284 | 120 | 164 | 3.5 | 0.7 |

Variation code: A(A ratio)-W(W ratio), FA: Fly ash dosage, AG: Total fine and coarse aggregate dosage, SS: Sodium silicate solution dosage, PSS: Pure SS dosage (water-less), SH: Sodium hydroxide solution dosage, PSH: Pure SH dosage (water-less), AA: Total activator solution (SS+SH), PA: Total pure activator dosage (PSS+PSH), PW: Pure water dosage, A ratio: SS/SH ratio, W ratio: AA/FA ratio

During the production of GPC specimens, commercially available river sand (0/4 mm), coarse basalt aggregate (7/14 mm), SS (modulus ratio of 2.06), and SH (14-M) were used. Table 2 shows the mixing dosage details of nine produced GPC variations. The additional calculated parameters in Table 2 provide investigate the A ratio (SS/SH), W ratio (AA/FA, where AA abbreviation is used for total alkaline activator dosage), total pure chemical activator dosage (PA), pure sodium silicate dosage (PSS), pure sodium hydroxide dosage (PSH), and pure water dosage (PW) effects, separately. Produced GPC variations in Table 2 were cast in 150x150x750 mm prism molds and cured at 90 °C for 24 hours. After de-molding, specimens were stored at room temperature for 28 days. Other information about the mix design, casting, and curing stages was presented in a previous study conducted by the authors [33]. Some of the produced prisms can be seen in Figure 3(a). These GPC prisms were first used for experimental modal tests and, after, were cut into 150x150x150 mm cubes (Figure 3(b)) for compressive strength tests.
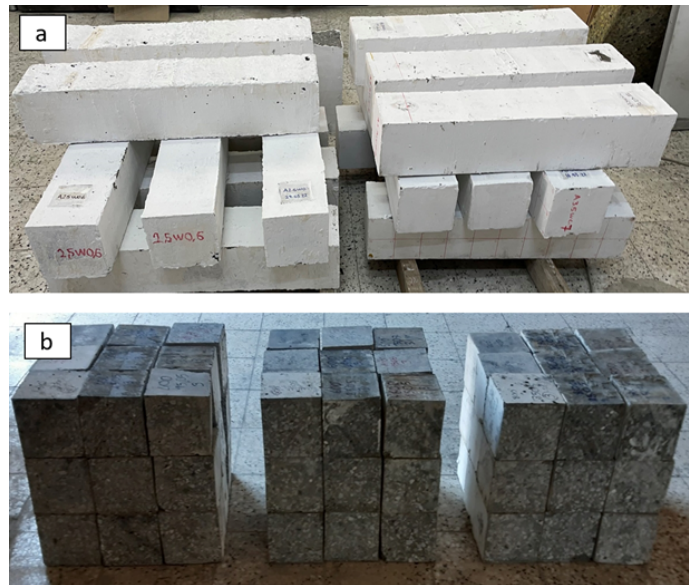


**Figure 3.** Produced 150x150x750 mm GPC prisms and 150x150x150 mm cubes obtained from these prisms.

## 3. Scanning Electron Microscope (SEM)-based Microstructural Analysis

This section will present scanning electron microscope (SEM) images for preliminary evaluations. Figures 4 to 7 present some SEM image examples for the A1.5-W0.5 and A3.5-W0.5 coded specimens. During analysis, SEM image examples of only these two variations were considered sufficient for this study, where the effects of chemical activators are investigated. These two variations were preferred since they contain an identically equal dosage of fly ash (406 kg/m$^3$), total aggregate dosage (AG) (1837 kg/m$^3$), and W ratio (0.5). Also, these variations contain identically equal total activator dosage (AA) (203 kg/m$^3$) and nearly equal pure water (PW) (117-120

kg/m$^3$) and pure activator (PA) (83-86 kg/m$^3$) dosages. The only difference between these variations is the chemical activator ingredients. While the A1.5-W0.5 coded specimens contain 29 kg/m$^3$ pure sodium hydroxide (PSH) and 54 kg/m$^3$ pure sodium silicate (PSS), the A3.5-W0.5 coded ones have 16 kg/m$^3$ and 70 kg/m$^3$, respectively. In the presented figures (Figures 4-7), unreacted (remained) FA particles, mullite crystallites (needle-shaped), and formless or spherical-shaped air voids (remain after reacted FA particles) are marked with descriptions for easy understanding.



**Figure 4.** An SEM image (left-upper-side) and magnified forms (zoomed into the yellow dashed circles) taken from an A1.5-W0.5 coded specimens.
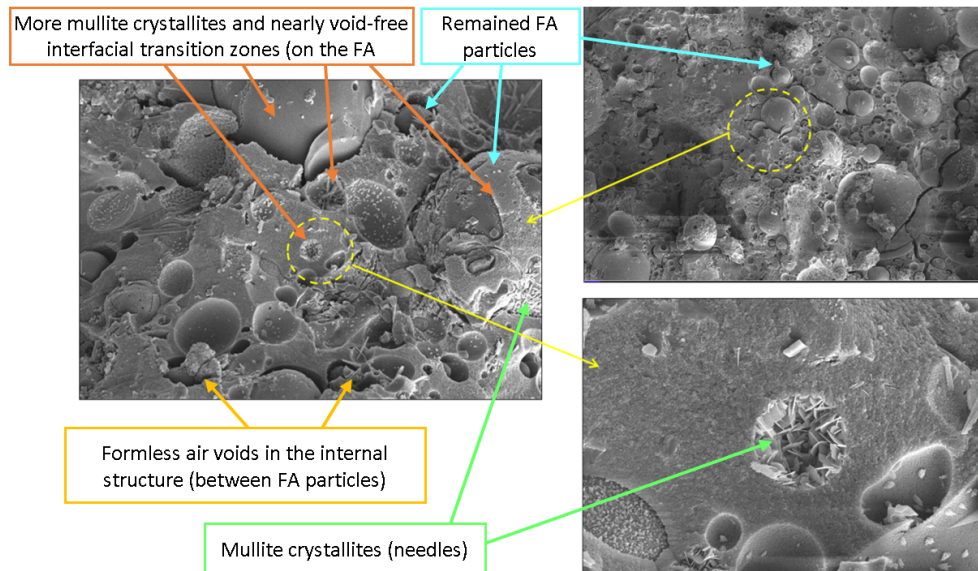


**Figure 5.** An SEM image (left-upper-side) and magnified forms (zoomed into the yellow dashed circles) taken from another A1.5-W0.5 coded specimens.
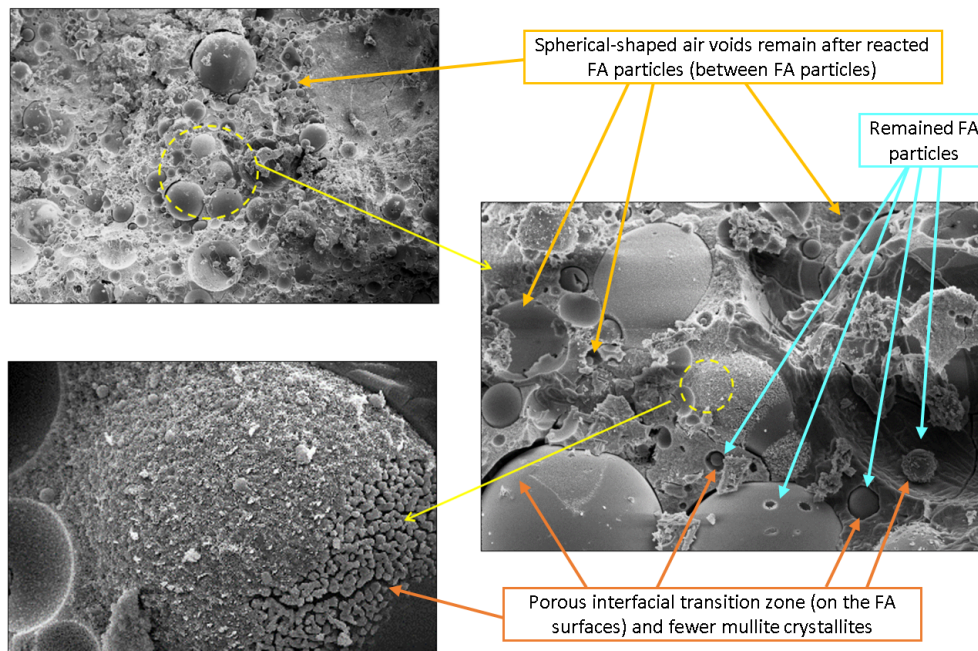
**Figure 6.** An SEM image (left-upper-side) and magnified forms (zoomed into the yellow dashed circles) taken from a A3.5-W0.5 coded specimens.
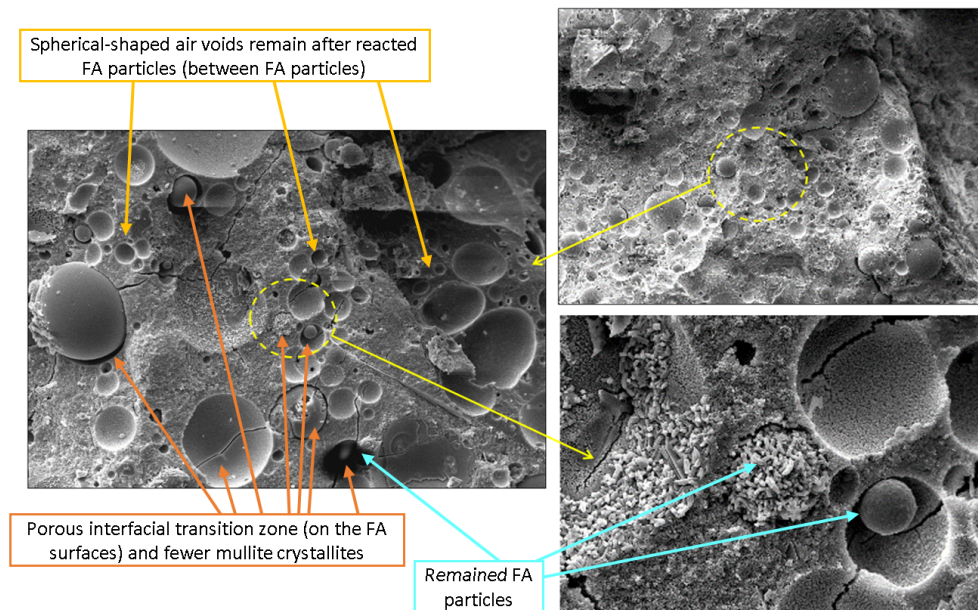


**Figure 7.** An SEM image (left-upper-side) and magnified forms (zoomed into the yellow dashed circles) taken from another A3.5-W0.5 coded specimens.

Figures 4 and 5 indicate a limited geopolymer development is in question, and a porous microstructure exists. Unreacted FA particles and shapeless air voids seen in these figures were effective in this evaluation. On the contrary, Figures 6 and 7 show that increasing the percentage of SS in the activator solution changes the microstructure. These figures show that FA particles are dissolved more or disappear completely, so a higher degree of geopolymer development is in question. In this condition, the shapeless air void-induced porosity between different FA particles was reduced with more geopolymer development, so a denser internal structure was observed. However, as seen from Figures 6 and 7, the spherical-shaped air void-induced porosity was

increased with more geopolymer development. On the other hand, porous interfacial transition zones on the FA surfaces (FA-ITZ) and fewer mullite crystallites were observed with increased SS in the activator solution.

The above findings are consistent with the other FA-based GPC studies [42-46] in the literature. However, these evaluations, like any other SEM analysis, are hypothetical and require several other investigation methods. From a superficial perspective, the SS activator may increase the static compressive strength and decrease the dynamic damping ratio as a result of a denser internal structure via the increasing geopolymer development characteristic. However, the effect of extra spherical voids and the porous FA-ITZ structure, described above, should also be addressed. These last differences may not decrease the compressive strength (mainly due to the increase in geopolymer development) and are more likely to contribute to damping. It is a matter of curiosity about what kind of situation will emerge at the end of the day. This issue will be further investigated with XRD-based microstructural, modal-based dynamic, and static compressive strength-based mechanical tests and analyses.

## 4. X-Ray Diffraction (XRD)-based Microstructural Analysis

This section will present X-Ray diffraction (XRD)-based analysis results for further microstructural evaluations. Figure 8 shows the XRD patterns of the A1.5-W0.5 and A3.5-W0.5 samples. These patterns were obtained by scanning the sample powders with X-rays. The selection of these two variants for XRD analysis is based on the same rationale as the SEM analysis described in the previous section. As seen in Figure 8, the XRD patterns of the GPC samples reveal a semi-crystalline structure (ranging from amorphous to semi-crystalline). These patterns and structural evaluations are consistent with other studies on low-calcium FA-based GPC samples [47-51]. In Figure 8, the highest intensity diffraction peaks correspond to quartz crystallites (a chemically and mechanically stable form of silicon dioxide, $SiO_2$), marked at 29.5° 2θ. Additionally, several other peaks related to different forms of silica are detected at 21°, 23°, 24°, 41°, 44°, 45°, 46°, and 51° 2θ. The second most abundant crystallite is mullite ($Al_6Si_2O_{13}$), observed at 27° and 31° 2θ. These crystallites are also prominent in the SEM images presented earlier (Figures 4 and 5) and align with previous findings. These phase determinations highlight the characteristics of low-calcium FA-based GPC and match other similar studies in the literature [47, 48, 52]. The total intensities of the mullite phases primarily come from unreacted FA particles that either remained or dissolved and rearranged during polymerization. In contrast, the total intensities of the silica phases result from a combination of river sand, unreacted FA particles, and new crystallites formed during polymerization.
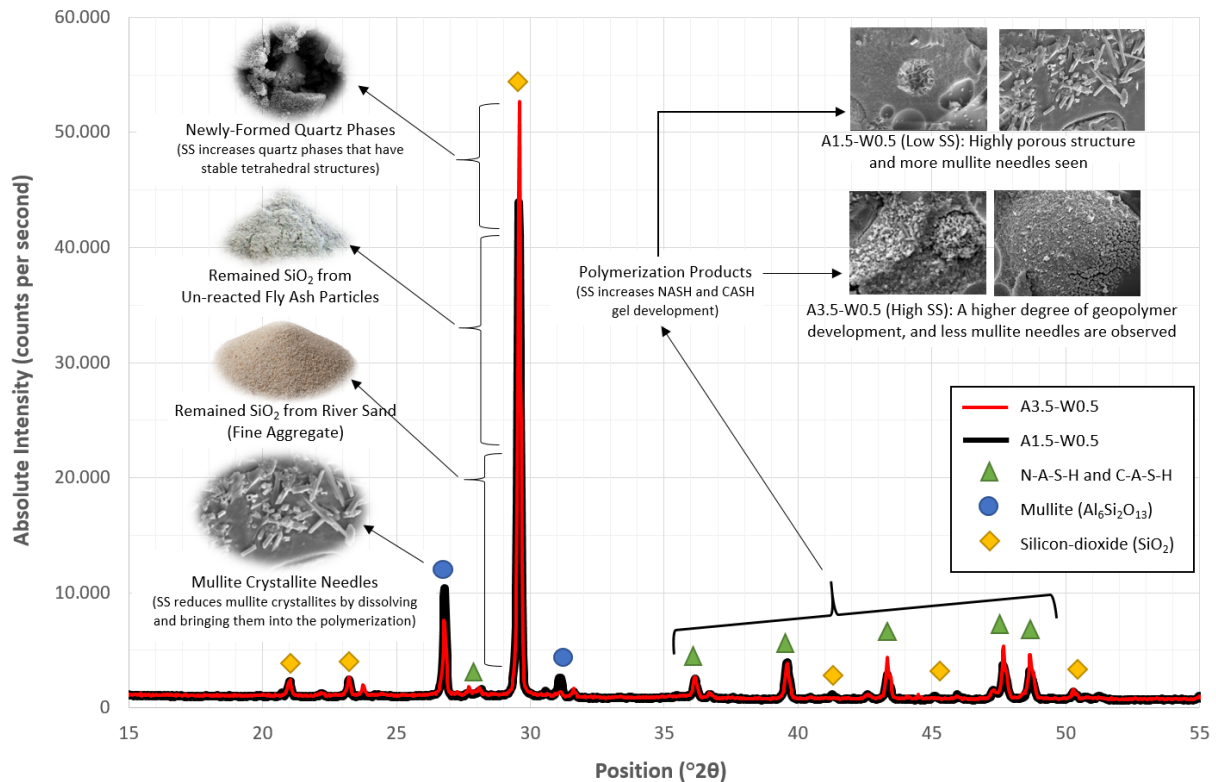


**Figure 8.** Comparison of the XRD patterns of A1.5-W0.5 and A3.5-W0.5 coded specimens.

For a better understanding of this subject, the components of each diffraction peak are described in Figure 8, and detailed interpretations by literature search are presented below:

Quartz and mullite crystallites are components of low-calcium FA and increase the crystallinity of FA-based GPC [47, 48]. However, because of their chemical stability, even if their intensities decrease with polymerization, some remain and do not react [47, 48]. These crystallites are demonstrated in Figure 8.

As reported in the literature [48, 50], newly- formed quartz phases (with stable tetrahedral structures) are observed if high-temperature curing is implemented, and these additional products contribute to compressive strength [48, 50]. These products and related phases are demonstrated in Figure 8.

Fine aggregates are used in the production of GPC. The river sand used in this study as fine aggregate is rich in Quartz crystallites [53, 54]. Hence, as seen in Figure 8, it has a considerable share in the quartz diffraction peak intensity of the XRD patterns, identified at 29.5° (2θ) for both variations.

Additionally, several peaks between 25-50° (2θ) are observed and determined as N-A-S-H or C-A-S-H. These phase determinations coincide with other similar studies in the literature [48, 50]. As stated in the literature, the major polymerization products and the main mechanical strength-providing elements of low-calcium FA-based GPC are the Sodium Aluminate Silicate Hydrate (N-A-S-H) gels [48, 55]. According to Fernández-Jiménez et al. [55], depending on the calcium content of FA, Calcium Aluminate Silicate Hydrate (C-A-S-H) gel products are also formed, albeit in much smaller amounts if low-calcium FA is used as the binder. These C-A-S-H products are also seen in OPC concrete and decrease the setting time of both concrete types [48].

The nature of the N-A-S-H and C-A-S-H gels depends on the type and dosage of the chemical activators [55] and increases with the polymerization degree [47, 48]. As seen in Figure 8, N-A-S-H or C-A-S-H phases were identified between 25-50° (2θ), and the diffraction peak intensities of A3.5-W0.5 were greater than A1.5-W0.5, indicating the reaction degree was better for this variation.

It is reported in the literature that SS activators promote the dissolution of solid crystallites (identified at 21, 23, 24, 27, 31, 41, 44, 45, 46 and 51° (2θ) for both of the variations), and bring them into polymerization [49]. As seen in Fig.8, most of the diffraction peak intensities of these phases are lower for the A3.5-W0.5 variation. On the other hand, the diffraction peak intensities of the N-A-S-H and C-A-S-H gels (identified between 25-50° 2θ) significantly enhanced. In other words, the solid contents in the A3.5-W0.5 dissolve higher, and more gel products are developed.

The above findings are consistent with the previously presented SEM image-based analyses and other XRD-based studies in the literature. However, like any other XRD-based microstructural analysis, these evaluations are hypothetical and require additional investigations. Therefore, this subject will be further investigated with modal-based dynamic and static compressive strength-based mechanical tests.

## 5. Modal Tests-based Dynamic Parameter Analysis

This section will present modal test and analysis results for experimental determination and evaluation of dynamic characteristic parameters. Figure 9 shows the modal test and analysis equipment used for these purposes in the previous study of the authors [33]. During these modal tests, a Dewe-43A-type USB DAQ system was used for the data acquisition. The analog sampling rate was selected as 10 kHz per channel. Produced GPC prism specimens (in Figure 3(a)) were placed on sufficiently soft urethane blocks, as suggested in the literature [56, 57], to provide a free vibrating condition. A compression-type Dytran 5800B2 model impulse hammer was used for the excitations. Each produced prism was divided into 33 equally distanced points. An IEPE shear type (MMF KS76C.100 model) accelerometer was mounted at each test specimen's corner point (33th point).

Each of the 33 points described above and shown in Figure 9 was excited five times with modal hammer strikes, and in the end, 165 FRF (frequency response spectrum) graphs were obtained for only a test specimen. After these, the resonance frequencies, damping ratios, and mode shape animations were obtained with the Dewesoft® Experimental Modal Analysis (EMA) software. During analysis, the mode indication functions (MIF) and modal circle methods are used in this study, as explained and suggested in the literature [58-60]. Figure 10 presents an example of resonance frequency and modal (viscous) damping ratio estimation. In this figure, MIF peak points near the value of one (1) indicate the resonance frequencies of the tested specimens [61], as values close to one in MIF graphs help identify the presence and frequency of resonance. Additionally, mode shape animations corresponding to each resonance frequency (first resonance, second resonance, etc.) are provided for easier understanding. Below the MIF graph in Figure 10, six modal circle analyses from one test specimen's endpoints are shown. The modal circles analysis method is one of the most common techniques for accurately determining damping ratios. The descriptions above these modal circles refer to the 'response point (33Z+)/excitation point (1Z+, etc.)' meanings.
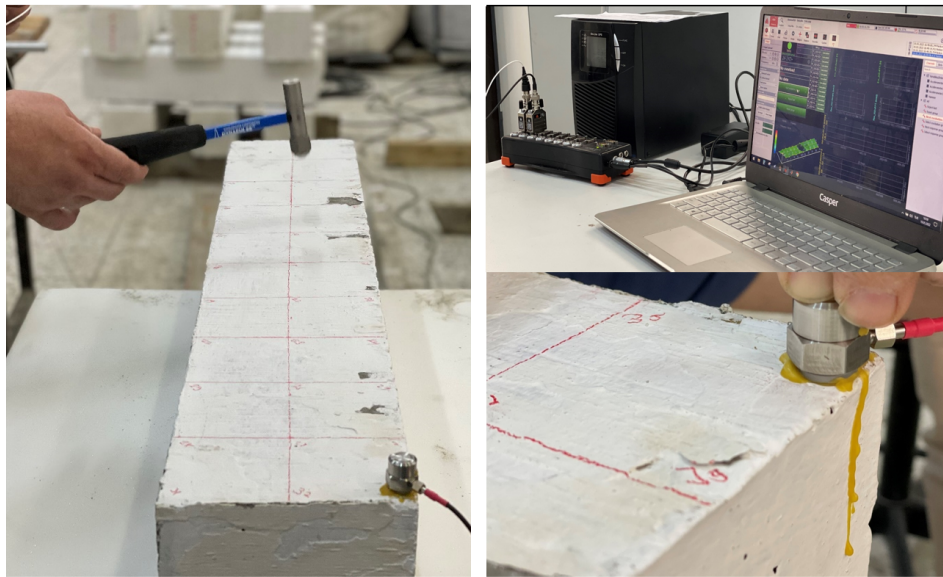
**Figure 9.** Produced 150x150x750 mm sized geopolymer concrete prisms and modal test setup [33].
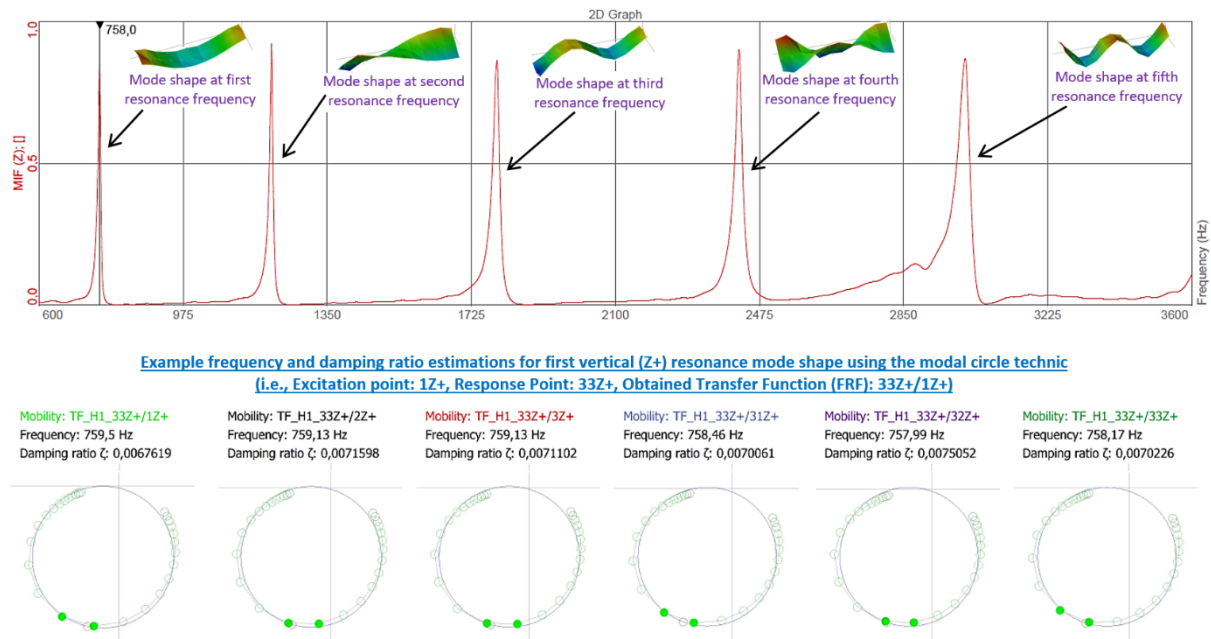


**Figure 10.** MIF graphs of an (A1.5-W0.7) test specimen (upper-side), and exact resonance frequency (Hz)-damping ratio (%) estimations using modal circle technique (down-side).

Table 3 summarizes the details of the obtained resonance frequencies, damping ratio values, and standard deviations. In the first column of Table 3, there are sample codes for which mix variation and component dosage (kg/m$^3$) information were given in Table 2 previously. In the second column, the first resonance frequency calculation results are presented. These frequencies were obtained with numerical averaging of the six modal circle analysis results, previously exemplified in Figure 10. The standard deviations of these resonant frequency values are given in the 3rd column of Table 3. Thanks to the applied test and analysis techniques, the standard deviations in the resonance frequency determinations are less than 1 per thousand. In the 4th column of Table 3, similarly determined damping ratio averages are given, and in the 5th column, the standard deviations of these values are

892

given. These deviation values can be interpreted as a success for modal testing, a non-destructive testing (NDT) method. These deviation values are even equal to or below the destructive static strength test limits.

**Table 3.** Modal analysis results

| Variation Code | Average First Resonance Frequency (Hz) | Resonance Frequency Standard Deviation | Average First Damping Ratio ($\zeta$) | Damping Ratio Standard Deviation |
|---|---|---|---|---|
| A1.5-W0.5 | 866.8 | 0.02% | 0.0059445 | 1.1% |
| A1.5-W0.6 | 803.2 | 0.03% | 0.0058477 | 2.4% |
| A1.5-W0.7 | 758.7 | 0.07% | 0.0070943 | 3.1% |
| A2.5-W0.5 | 840.7 | 0.06% | 0.0061537 | 1.8% |
| A2.5-W0.6 | 820.0 | 0.04% | 0.0069172 | 2.0% |
| A2.5-W0.7 | 783.7 | 0.08% | 0.0070373 | 5.3% |
| A3.5-W0.5 | 843.9 | 0.02% | 0.0052906 | 0.7% |
| A3.5-W0.6 | 802.3 | 0.05% | 0.0059717 | 1.8% |
| A3.5-W0.7 | 744.9 | 0.09% | 0.0072020 | 2.2% |

Figure 11 shows the relationships between pure water dosage (PW), damping ratio, and resonance frequency. As stated in the literature [55] and deduced after previously presented XRD-based microstructural analysis, the nature of the N-A-S-H and C-A-S-H gels depends on the type and dosage of the chemical activators. Therefore, during the preparation of Figure 11, after testing many alternatives, it was concluded that "categorizing the produced GPC variations based on the A ratio of each variation" provides more meaningful results. As observed, the dynamic characteristics of GPC variations are closely linked to the water content (PW). Generally, increasing PW leads to higher damping ratios (a positive correlation) and lower resonance frequencies (a negative correlation). As mentioned earlier, this behavior in GPC is similar to that of OPC concrete [33]. While numerically comparing the dynamic performances of different concrete types is beyond the scope of this study, it is likely that the effect of PW is more pronounced in GPC. This is because, as noted in the literature, water is only minimally consumed during the geopolymerization process [62].

Another issue that must be investigated is that the liquid ingredients of GPC also contain chemical activators. Figure 12 shows the relationships between these chemical activators, damping ratio, and resonance frequency. During the preparation of this figure, the effects of pure sodium silicate (PSS), pure sodium hydroxide (PSH), and the sum of these activators (PA) were investigated separately. As deduced from Figure 12, increasing these parameters has an increasing effect on modal damping ratios (positive correlation) and decreasing effect on resonance frequencies (negative correlation).

After these, the linear regression coefficients of determination ($R^2$) values, calculated and presented in Figures 11 and 12, will be evaluated. As deduced from these figures, the resonance frequencies show a stronger correlation than the damping ratios. It is undeniable that the damping ratios of structures composed of heterogeneous materials like GPC or OPC concrete may differ somewhat throughout the entire cross-section. Conversely, every resonant frequency across the cross-section should remain consistent [33]. Therefore, during analysis, all sections of a specimen are expected to vibrate at uniform frequencies, except at nodal points. However, the test samples in question do not have a homogeneous structure with the same mass and modulus of elasticity at every location. On the other hand, some excitations may coincide near or on the aggregate grains. So, it is impossible to talk about precise damping ratio detection throughout the entire section. This deviation during modal damping estimations is also more or less valid for other mechanical and microstructural tests and analyses. However, utilizing several advanced modal analysis techniques, the maximum deviation value was kept chiefly below 5%, preventing further increases due to test and analysis imperfections. These slight deviations obtained by non-destructive (NDT) modal tests are even lower than the standard deviation levels commonly accepted for static concrete strength tests. When continuing these analyses, it can be deduced from Figure 11 that the PW dosage showed a strong correlation. On the other hand, in Figure 12, the SS dosage has a higher correlation with the modal parameters than the SH dosage. It is a fact that the effect of liquid ingredients (chemical activators and water) is more complex for GPC compared to OPC concrete. Because as the liquid activator solution dosages of the GPC (SS and SH) increase, the increasing pure chemical contents (PSS and PSH) promote more geopolymer development. At the same time, increasing pure water content (PW) increases porosity.
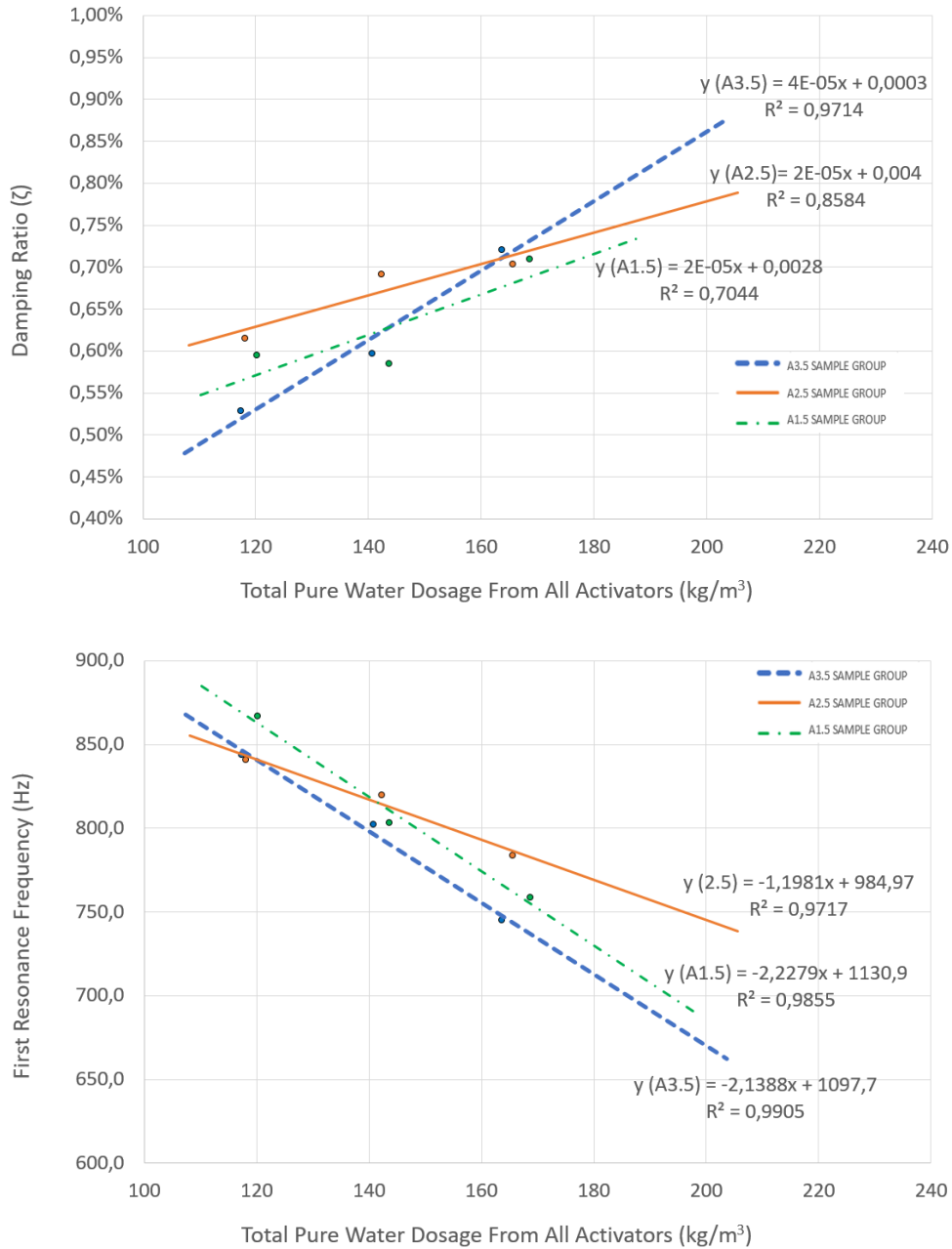
**Figure 11.** Effect of the pure water dosage (PW) on the modal parameters (damping ratio (upper-side) and resonance frequency (down-side)) of specimens categorized into the A ratio groups.
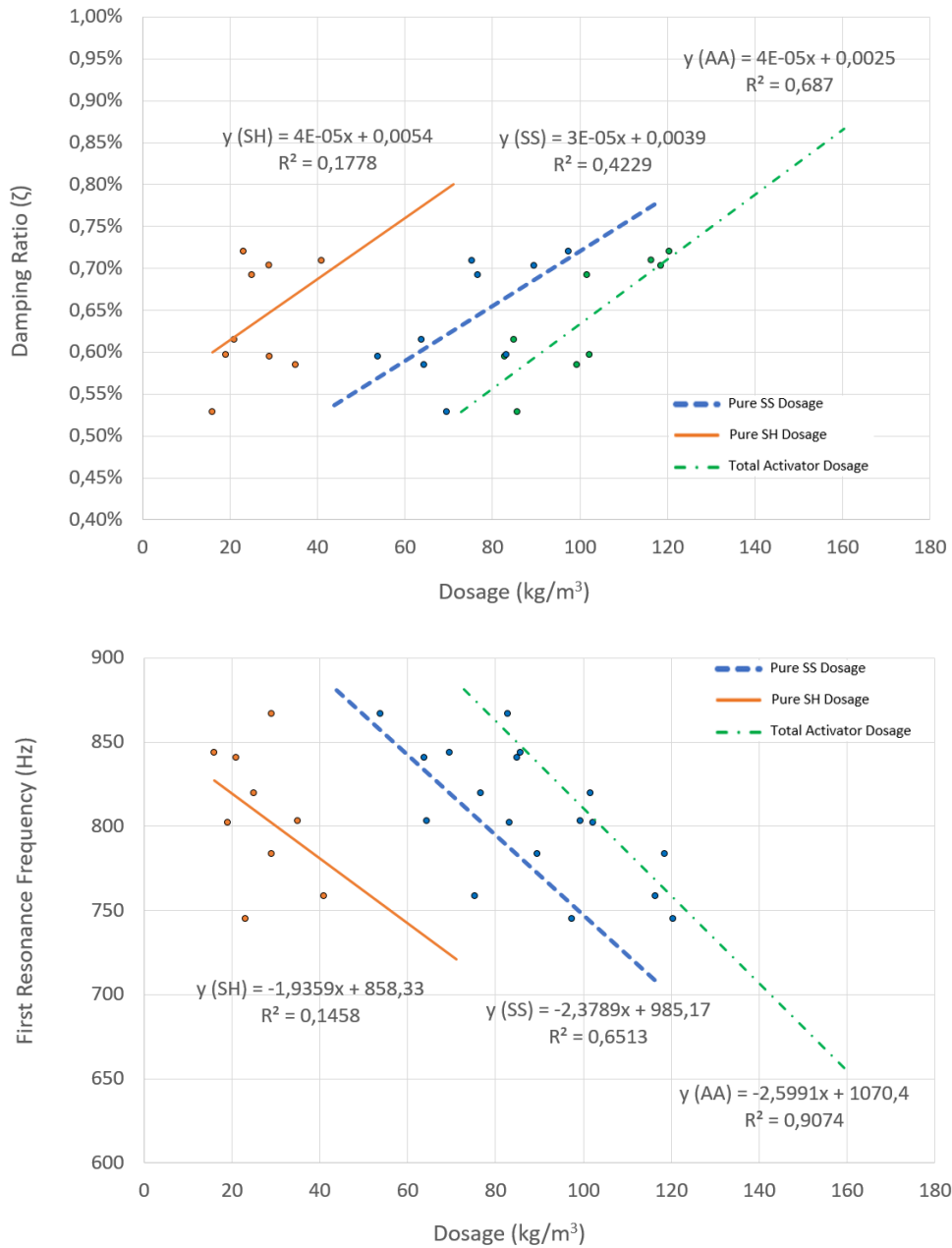
**Figure 12.** Effect of the pure activator dosages on the modal parameters (damping ratio (upper-side) and resonance frequency (down-side)) of specimens.

## 6. Static Compressive Strength Tests- Based Analysis

This section will present experimental mechanical test results for determining and evaluating the static compressive strength characteristics of the produced GPC variations. For these purposes, the 150x150x750 mm sized prisms (in Figure 3(a)) previously used for modal tests were cut into cubes of 15 cm (in Figure 3(b)) and subjected to compressive strength tests. Figure 13 shows the results of these tests, with the previously presented modal analysis results. Depending on their placement in the appropriate column and category, bar graphs in this image illustrate the numerical values in each line. In Figure 13, GPC variations have been subjected to the "A ratio-based categorization." Because as stated in the literature [55] and deduced after previously presented XRD-based microstructural analysis and experimental modal analysis, the nature of the N-A-S-H and C-A-S-H gels

depends on the type and dosage of the chemical activators. Therefore, during the preparation of Figure 13, after testing many alternatives, it was concluded that investigating the produced GPC variations based on the A ratio provides more meaningful results.

| Variation Code | A Ratio Category | Average Compressive Strength (MPa) | Average First Resonance Frequency (Hz) | Average First Damping Ratio (ζ) |
|---|---|---|---|---|
| A1.5-W0.5 | 1.5 | 35,5 | 866,8 | 0,005945 |
| A1.5-W0.6 | 1.5 | 39,5 | 803,2 | 0,005848 |
| A1.5-W0.7 | 1.5 | 40,4 | 758,7 | 0,007094 |
| A2.5-W0.5 | 2.5 | 39,2 | 840,7 | 0,006154 |
| A2.5-W0.6 | 2.5 | 39,8 | 820,0 | 0,006917 |
| A2.5-W0.7 | 2.5 | 42,3 | 783,7 | 0,007037 |
| A3.5-W0.5 | 3.5 | 47,8 | 843,9 | 0,005291 |
| A3.5-W0.6 | 3.5 | 48,4 | 802,3 | 0,005972 |
| A3.5-W0.7 | 3.5 | 49,7 | 744,9 | 0,007202 |

**Figure 13.** Demonstration of the static compressive strength and dynamic (modal) parameters of the produced variations using bar graphs.

Figure 14 shows the relationships between the total pure alkaline activator dosage from all chemical solutions (PA) and compressive strengths. During the preparation of this figure, as previously deduced, the "A ratio-based categorization method" was used. Coupled with the findings of Figure 13, it can be concluded that increasing the A ratio and PA has an increasing effect on compressive strength values.
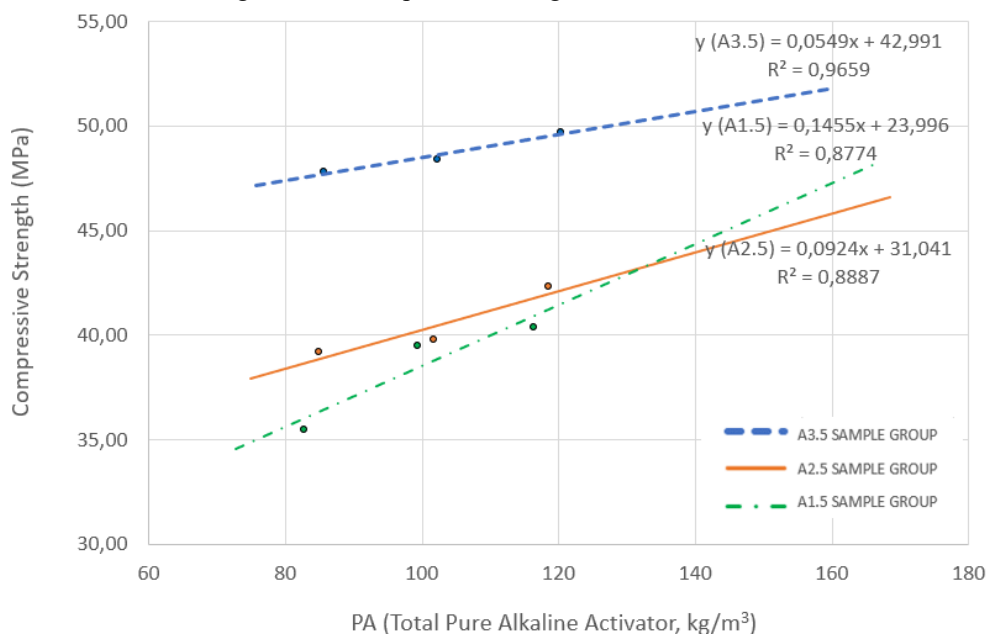


**Figure 14.** Effect of the PA dosages on the strengths of specimens categorized into the A ratio groups.

Figures 15 and 16 show the relationships between the dynamic and static characteristic parameters obtained at the end of all these tests and analyses. During the preparation of these figures, as previously deduced, the "A ratio-based categorization method" was used. When comparing the regression coefficient of determination ($R^2$) values, the resonance frequencies show a stronger relationship than the damping ratios. The reasons were explained

in detail in the fifth section. The heterogeneity of GPC specimens seems to affect the damping and static strength more than the resonance frequency characteristics. This prediction is logical since a test sample under vibration should all oscillate with the same resonance frequencies except for its nodal points. However, since the specimens in question do not have a homogeneous structure at every location, it is nearly impossible to talk about the same microstructure, damping ratio, or compressive strength detection throughout the entire section.
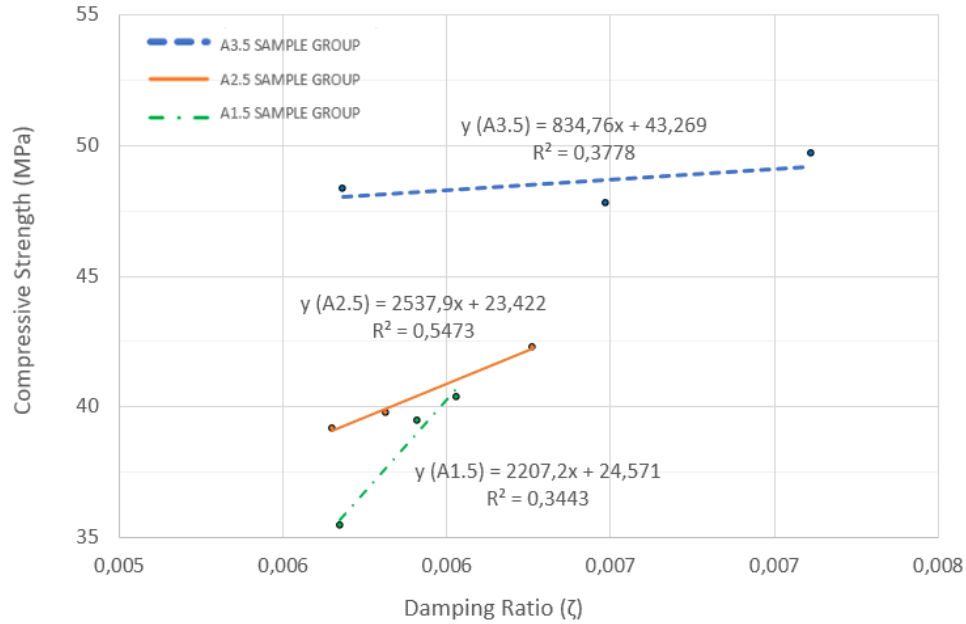
**Figure 15**. Compressive strength and damping ratio relationships.
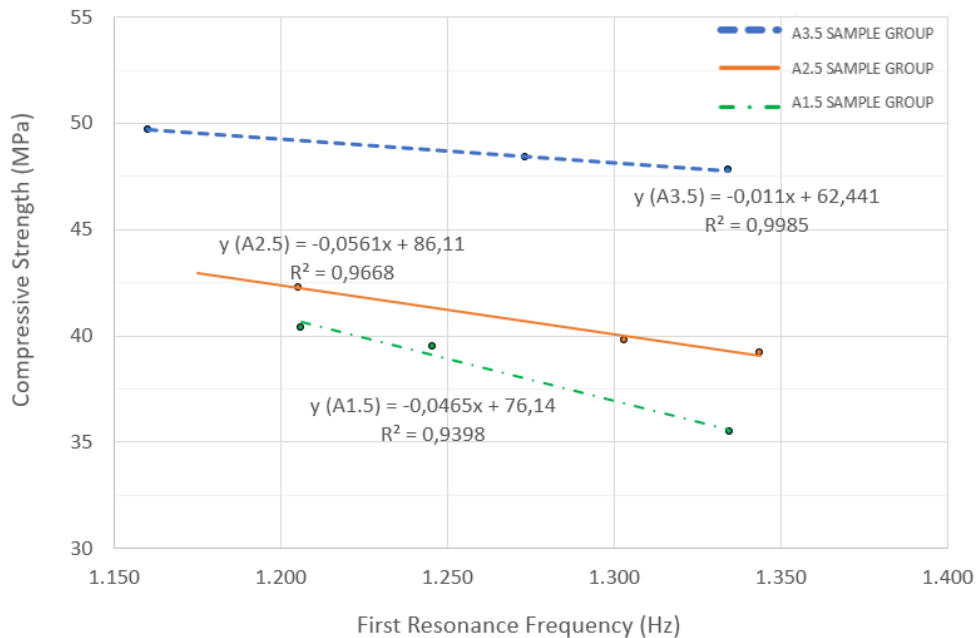
**Figure 16.** Compressive strength and resonance frequency relationships.

To sum up, most buildings and structures inevitably experience dynamic loadings today. Therefore, the dynamic characteristics and damping behaviors of structural materials are, at least, just as important as their static capacities. Hence, today, engineers need co-currently increase the dynamic damping ratios and static compressive strengths of concrete materials. However, as concluded from the presented literature review, as the static strength

of OPC concrete increases, its dynamic damping ratio generally decreases. Today, the co-currently increasing dynamic damping ratio and static compressive strength of OPC concrete material are still challenges to overcome. These comparisons are made based on the reciprocal changing behaviors of static and dynamic performances. Numerically comparing the dynamic performances and enhancement methods of OPC concrete with other concrete types, i.e., geopolymer concrete, is excluded from the scope of this study. Because it is more reasonable to say that geopolymer concrete and OPC concrete are made using fairly different procedures and that both materials have unique and specific dynamic performance enhancing strategies, as mentioned by the authors in a prior study [26].

Several investigations on OPC concrete demonstrate that an increased water/cement ratio results in a reduction in strength but an increase in damping ratio [14, 63]. It is valid for both; GPC and OPC concrete; a porous structure (water-filled or empty voids) causes an increase in the damping ratios. Dynamic stress waves undergo more refraction and damping in these porous structures. But the decisive factor for the mechanical strengths is when the liquid content in both of these materials (GPC and OPC concrete) increases, while a porous formation that negatively affects the strength occurs in OPC; in GPC, this porosity develops in a way that does not adversely affect the mechanical strength [64]. Or it can be expressed as follows, the increase in strength due to the increase in geopolymer development is at a level that can prevent the strength from decreasing due to the additional porous structure. As deduced from the presented test and analysis results, in the studied analysis range, as the static compressive strength values increase, generally, the damping ratios increase (positive correlation), and the resonance frequencies decrease (negative correlation). This behavior should be noted as an essential difference distinguishing GPC from OPC concrete. However, the SS activator's regression coefficients of determination were considerably higher than the SH's. In this sense, if the pure sodium silicate dosages (PSS) of the designed specimens are increased from 55 kg/m$^3$ to 98 kg/m$^3$ gradually, the damping ratios increase continuously and show a percentage increase of 17% in the final dosage (seen in Figure 12). Under the same conditions, resonance frequencies show a 12% reduction (seen in Figure 12). At an exciting point, under the same conditions, the compressive strength values also increase in parallel with the damping ratio. This percentage increase reaches 39% in the final dosage (seen in Figures 15 and 16).

## 7. Conclusions and Future Prospects

This study investigates the co-relationship between the damping and compressive strength of heat-cured low-calcium fly ash-based geopolymer concrete (GPC) variations produced with variable sodium silicate (SS) and hydroxide (SH) activators. According to the modal, mechanical, and microstructural tests and analyses, the following findings have been obtained:

- According to the modal test and analysis results, the damping ratios of specimens generally increase with the increase of the SS and SH dosages. However, the SS activator's regression coefficients of determination were considerably higher than the SH's.

- According to the SEM image and XRD-based microstructure analysis, the fly ash (FA) particles dissolve and react more as the chemical activators increase. A specific porosity is observed. The dynamic stress waves are predicted to undergo more refraction and damping because of the specific porous structure mentioned above. In this aspect, the SS activator showed a higher effect and stronger correlation than the SH.

- According to the compressive strength test results, despite the mentioned specific porous structure, surprisingly, strength values also co-currently increase with the increase of the SS and SH dosages.

- Coupled with the modal test and analysis results, positive correlations between the static compressive strength and dynamic damping ratio were determined for the variable pure sodium hydroxide (PSH) and pure sodium silicate (PSS) dosages. In this aspect, the PSS values showed a higher effect and stronger correlation than the PSH.

- In ordinary Portland cement (OPC) concretes, a higher water/cement ratio increases damping but reduces strength. In GPC, more water from liquid activators increases porosity. However, it also increases the PSS and hence the degree of polymerisation. Eventually, as the strength improves enough to offset the negative effects of increased porosity, both damping and strength values increase together.

- The $R^2$ values in Figures 11, 12, 15 and 16 show that resonant frequencies have a stronger correlation with dynamic and static characteristic parameters than damping ratios. This is because heterogeneity in materials such as GPC or OPC concrete affects damping and static strength more than resonant frequency properties. While resonant frequencies remain consistent across the cross section, variations in microstructure, damping ratios and compressive strength are inevitable.

- As the PSS dosage increased from 55 kg/m³ to 98 kg/m³, the modal damping ratios increased steadily, reaching a 17% increase at the final dosage. In contrast, the resonant frequencies, which showed a stronger correlation, decreased by 12%. Interestingly, the compressive strength also increased with the damping ratio, with a final percentage increase of 39%.

These presented findings are expected to be beneficial for engineers and researchers. With these analyses, the benefits of appropriately and eco-effectively using this newly developed material are better revealed, and its widespread use is encouraged. It would be advantageous to carry out more research on the topic using other kinds of geopolymer concrete and a wider variety of mixing ratios.

## Acknowledgments

## References

[1] Remennikov AM, Kaewunruen S. A review of loading conditions for railway track structures due to train and track vertical interaction. Struct Control Health Monit 2008; 15(2): 207-234.

[2] Cui Y, Hao H, Li J, Chen W. Effect of adding methylcellulose on mechanical and vibration properties of geopolymer paste and hybrid fiber-reinforced geopolymer composite. J Mater Civ Eng 2020; 32(7): 04020166.

[3] Ou J, Liu T, Li J. Dynamic and seismic property experiments of high damping concrete and its frame models. Journal of Wuhan University of Technology-Mater Sci Ed 2008; 23(1): 1-6.

[4] Shah AA, Ribakov Y. Recent trends in steel fibered high-strength concrete. Mater Des 2011; 32(8-9): 4122-4151.

[5] Hadi MNS, Li J. External reinforcement of high strength concrete columns. Compos Struct 2004; 65(3-4): 279-287.

[6] Tayeh BA, Bakar BA, Johari MM, Voo YL. Mechanical and permeability properties of the interface between normal concrete substrate and ultra high performance fiber concrete overlay. Constr Build Mater 2012; 36: 538-548.

[7] Salman MM, Al-Amawee AH. The ratio between static and dynamic modulus of elasticity in normal and high strength concrete. Journal of Engineering and Sustainable Development 2006; 10(2): 163-174.

[8] Alexa-Stratulat SM, Mihai P, Toma AM, Taranu G, Toma IO. Influence of Concrete Strength Class on the Long-Term Static and Dynamic Elastic Moduli of Concrete. Applied Sciences 2021; 11(24): 11671.

[9] Zahid MM, Bakar BA, Nazri FM, Ab Rahim MA. A review on raw materials and curing methods applied in production of ultra high performance concrete. In: IOP Conference Series: Materials Science and Engineering 2020; p. 012202.

[10] Ferdous W, Manalo A, Van Erp G, Aravinthan T, Kaewunruen S, Remennikov A. Composite railway sleepers–Recent developments, challenges and future prospects. Compos Struct 2015; 134: 158-168.

[11] Aktaş B, Cecen F, Öztürk H, Navdar MB, Öztürk İŞ. Comparison of prestressed concrete railway sleepers and new LCR concrete sleepers with experimental modal analysis. Eng Fail Anal 2022; 131: 105821.

[12] Lu JX, Shen P, Ali HA, Poon CS. Mix design and performance of lightweight ultra-high-performance concrete. Mater Des  2022; 216: 110553.

[13] Liang C, Liu T, Xiao J, Zou D, Yang Q. The damping property of recycled aggregate concrete. Constr Build Mater 2016; 102: 834-842.

[14] Tian Y, Shi S, Jia K, Hu S. Mechanical and dynamic properties of high strength concrete modified with lightweight aggregates presaturated polymer emulsion. Constr Build Mater 2015; 93: 1151-1156.

[15] Zeitouni AI, Rizos DC, Qian Y. Benefits of high strength reduced modulus (HSRM) concrete railroad ties under center binding support conditions. Constr Build Mater 2018; 192: 210-223.

[16] Giner VT, Baeza FJ, Ivorra S, Zornoza E, Galao Ó. Effect of steel and carbon fiber additions on the dynamic properties of concrete containing silica fume. Mater Des 2012; 34: 332-339.

[17] Fu X, Chung DD. Vibration damping admixtures for cement. Cem Concr Res 1996; 26(1): 69-75.

[18] Meesit R, Kaewunruen S. Vibration characteristics of micro-engineered crumb rubber concrete for railway sleeper applications. J Adv Concr Technol 2017; 15(2): 55-66.

[19] Sukontasukkul P. Use of crumb rubber to improve thermal and sound properties of pre-cast concrete panel. Constr Build Mater 2009; 23(2): 1084-1092.

[20] Zhou C, Pei X, Li W, Liu Y. Mechanical and damping properties of recycled aggregate concrete modified with air-entraining agent and polypropylene fiber. Materials 2020; 13(8): 2004.

[21] Giner VT, Ivorra S, Baeza FJ, Zornoza E, Ferrer B. Silica fume admixture effect on the dynamic properties of concrete. Constr Build Mater 2011; 25(8): 3272-3277.

[22] Warburton GB. The Dynamical Behaviour of Structures. 2nd Edition. New York: PERGAMON PRESS OXFORD, ISBN: 9781483187785, 1976.

[23] Swamy N, Rigby G. Dynamic properties of hardened paste, mortar and concrete. Matériaux et construction 1971; 4: 13-40.

[24] Salzmann, A. Damping characteristics of reinforced and prestressed normal-and high-strength concrete beams. Griffith University, 2003.

[25] Eiras JN, Popovics JS, Borrachero MV, Monzó J, Payá J. The effects of moisture and micro-structural modifications in drying mortars on vibration-based NDT methods. Constr Build Mater 2015; 94: 565-571.

[26] Provis JL, Brice DG, Buchwald A, Duxson P, Kavalerova E, Krivenko PV, Wiercx JALM. Demonstration projects and applications in building and civil infrastructure. Alkali Activated Materials: State-of-the-Art Report, RILEM TC 224-AAM 2014; 309-338.

[27] Amran YM, Alyousef R, Alabduljabbar H, El-Zeadani M. Clean production and properties of geopolymer concrete; A review. Cleaner Prod 2020; 251: 119679.

[28] Bondar, D. Geo-polymer concrete as a new type of sustainable construction materials. In: Proceedings of the Third International Conference on Sustainable Construction Materials and Technologies (ICSCMT) 2013; 18-21.

[29] Guo X, Shi H, Dick WA. Compressive strength and microstructural characteristics of class C fly ash geopolymer. Cem Concr Compos 2010; 32(2): 142-147.

[30] Khan MZN, Hao Y, Hao H, Shaikh FUA. Mechanical properties of ambient cured high strength hybrid steel and synthetic fibers reinforced geopolymer composites. Cem Concr Compos 2018; 85: 133-152.

[31] Pan Z, Feng KN, Gong K, Zou B, Korayem AH, Sanjayan J, Collins F. Damping and microstructure of fly ash-based geopolymers. J Mater Sci 2013; 48: 3128-3137.

[32] Özbayrak A, Kucukgoncu H, Atas O, Aslanbay HH, Aslanbay YG, Altun F. Determination of stress-strain relationship based on alkali activator ratios in geopolymer concretes and development of empirical formulations. Structures 2023; 2048-2061.

[33] Cecen F, Özbayrak A, Aktaş B. Experimental modal analysis of fly ash-based geopolymer concrete specimens via modal circles, mode indication functions, and mode shape animations. Cem Concr Compos 2023; 137: 104951.

[34] Okoye FN, Durgaprasad J, Singh NB. Effect of silica fume on the mechanical properties of fly ash based-geopolymer concrete. Ceram Int   2016; 42(2): 3000-3006.

[35] Farooq F, Jin X, Javed MF, Akbar A, Shah MI, Aslam F, Alyousef R. Geopolymer concrete as sustainable material: A state of the art review. Constr. Build. Mater. 2021; 306: 124762.

[36] Gupta P, Nagpal G, Gupta N. Fly ash-based geopolymers: an emerging sustainable solution for heavy metal remediation from aqueous medium. Beni-Suef University Journal of Basic and Applied Sciences 2021; 10(1): 89.

[37] Temuujin J, Minjigmaa A, Bayarzul U, Kim DS, Lee SH, Lee HJ, MacKenzie KJD. Properties of geopolymer binders prepared from milled pond ash. Materiales de Construccion 2017; 67(328): 134.

[38] Acar MC, Şener A, Özbayrak A, Çelik Aİ. Geopolimer Harçlarda Zeolit Katkisinin Etkisİ. Mühendislik Bilimleri ve Tasarım Dergisi 2020; 8(3): 820-832.

[39] Bernal SA, Provis JL. Durability of alkali-activated materials: progress and perspectives. J Am Ceram Soc 2014; 97(4): 997-1008.

[40] Adak D, Mandal S.  Strength and durability performance of fly ash–based process-modified geopolymer concrete. J Mater Civ Eng 2019; 31(9): 04019174.

[41] Özbayrak A, Kucukgoncu H, Aslanbay HH, Aslanbay YG. Atas O. Comprehensive experimental analysis of the effects of elevated temperatures in geopolymer concretes with variable alkali activator ratios, J Build Eng 2023; 68: 106108.

[42] Luna-Galiano Y, Fernández-Pereira C, Izquierdo M. Contributions to the study of porosity in fly ash-based geopolymers. Relationship between degree of reaction, porosity and compressive strength. Mater Constr 2016; 66(324): 098.

[43] Ma Y, Hu J, Ye G. The effect of activating solution on the mechanical strength, reaction rate, mineralogy, and microstructure of alkali-activated fly ash. J Mater Sci 2012; 47: 4568-4578.

[44] Brough AR, Atkinson A. Sodium silicate-based, alkali-activated slag mortars: Part I. Strength, hydration and microstructure. Cem Concr Res 2002; 32(6): 865-879.

[45] Çelik Aİ, Tunç U, Bahrami A, Karalar M, Mydin MAO, Alomayri T, Özkılıç YO. Use of waste glass powder toward more sustainable geopolymer concrete. J Mater Res Technol 2023; 24: 8533-8546.

[46] Özkılıç YO, Çelik Aİ, Tunç U, Karalar M, Deifalla A, Alomayri T, Althoey F. The use of crushed recycled glass for alkali activated fly ash based geopolymer concrete and prediction of its capacity. J Mater Res Technol 2023; 24: 8267-8281.

[47] Huang W, Wang H. Geopolymer pervious concrete modified with granulated blast furnace slag: Microscale characterization and mechanical strength. J Cleaner Prod 2021; 328: 129469.

[48] Xiao R, Ma Y, Jiang X, Zhang M, Zhang Y, Wang Y, He Q. Strength, microstructure, efflorescence behavior and environmental impacts of waste glass geopolymers cured at ambient temperature. J Cleaner Prod 2020; 252: 119610.

[49] Huo W, Zhu Z, Sun H, Gao Q, Zhang J, Wan Y, Zhang C. Reaction kinetics, mechanical properties, and microstructure of nano-modified recycled concrete fine powder/slag based geopolymers. J Cleaner Prod 2022; 372: 133715.

[50] Zhang Y, Xiao R, Jiang X, Li W, Zhu X, Huang B. Effect of particle size and curing temperature on mechanical and microstructural properties of waste glass-slag-based and waste glass-fly ash-based geopolymers. J Cleaner Prod 2020; 273: 122970.

[51] Zhang Y, Xiao R, Jiang X, Li W, Zhu X, Huang B. Effect of particle size and curing temperature on mechanical and microstructural properties of waste glass-slag-based and waste glass-fly ash-based geopolymers. J Cleaner Prod 2020; 273: 122970.

[52] Han G, Yang S, Peng W, Huang Y, Wu H, Chai W, Liu J. Enhanced recycling and utilization of mullite from coal fly ash with a flotation and metallurgy process. J Cleaner Prod 2018; 178: 804-813.

[53] Xu W, Wen X, Wei J, Xu P, Zhang B, Yu Q, Ma H. Feasibility of kaolin tailing sand to be as an environmentally friendly alternative to river sand in construction applications. J Cleaner Prod 2018; 205: 1114-1126.

[54] Zhou N, Zhang J, Ouyang S, Deng X, Dong C, Du E. Feasibility study and performance optimization of sand-based cemented paste backfill materials. J Cleaner Prod 2020; 259: 120798.

[55] Fernández-Jiménez A, Palomo A, Criado M. Microstructure development of alkali-activated fly ash cement: a descriptive model. Cem Concr Res 2005; 35(6): 1204-1209.

[56] Çeçen F, Aktaş B. Modal and harmonic response analysis of new CFRP laminate reinforced concrete railway sleepers. Eng. Fail. Anal. 2021; 127: 105471.

[57] Aktaş B, Cecen F, Öztürk H, Navdar MB, Öztürk İŞ. Comparison of prestressed concrete railway sleepers and new LCR concrete sleepers with experimental modal analysis. Eng Fail Anal 2022; 131: 105821.

[58] Gjelstrup SL. What is modal analysis: the ultimate guide. DEWESoft, Available: https://dewesoft. com/daq/what-is-modal-analysis. [Accessed 11 06 2022], 2021.

[59] Irretier HD. History and development of frequency domain methods in experimental modal analysis. J Phys 2002; 12(11): 11-91.

[60] Avitabile P. Modal space-in our own little world. Exp Tech 2013; 37: 4-6.

[61] Modal Test and Modal Analysis, https://training.dewesoft.com/online/course/modal-testing-frf#mode-indicator-function-mif, Accessed 14.09.2024

[62] Šmilauer V, Hlaváček P, Škvára F, Šulc R, Kopecký L, Němeček J. Micromechanical multiscale model for alkali activation of fly ash and metakaolin. J Mater Sci 2011; 46: 6545-6555.

[63] Tian Y, Lu D, Zhou J, Yang Y, Wang Z. Damping property of cement mortar incorporating damping aggregate. Materials 2020; 13(3): 792.

[64] Aslanbay YG, Aslanbay HH, Özbayrak A, Kucukgoncu H, Atas O. Comprehensive analysis of experimental and numerical results of bond strength and mechanical properties of fly ash based GPC and OPC concrete. Constr Build Mater 2024; 416: 135175.